AD-A062 931 HARRY DIAMOND LABS ADELPHI MD F/G 20/7
AURORA ELECTRON BEAM MODIFICATION.(U)
JUL 78 S E GRAYBILL
UNCLASSIFIED HDL-TR-1862 NL

| OF |
AD
A062931

END
DATE
FILMED
3-79
DDC

where Z_0 is the characteristic impedance of the coaxial line, for radially emitted electrons from the inner conductor of the coaxial line to be trapped inside the outer conductor and be swept downstream. If this magnetic insulation is not present, the entire current output of the pulser can be shunted off through field emission in the coaxial lines. The 45-deg bend in the coaxial line reduces the magnetic field by about 30 percent and puts severe limits on the gap impedance.

It is shown in the appendix that the turnaround distance, r, of a

UNCLASSIFIED
SECURITY CLASSIFICATION OF THIS PAGE (When Data Entered)

REPORT DOCUMENTATION PAGE

READ INSTRUCTIONS BEFORE COMPLETING FORM

(14) 1. REPORT NUMBER: HDL-TR-1862
2. GOVT ACCESSION NO.
3. RECIPIENT'S CATALOG NUMBER

(6) 4. TITLE (and Subtitle): AURORA Electron Beam Modification.
(9) 5. TYPE OF REPORT & PERIOD COVERED: Technical Report.
6. PERFORMING ORG. REPORT NUMBER

(10) 7. AUTHOR(s): Stewart E. Graybill
8. CONTRACT OR GRANT NUMBER(s)

9. PERFORMING ORGANIZATION NAME AND ADDRESS
Harry Diamond Laboratories
2800 Powder Mill Road
Adelphi, MD 20783

10. PROGRAM ELEMENT, PROJECT, TASK AREA & WORK UNIT NUMBERS
Prog. element: 6.27.10H

(11) 11. CONTROLLING OFFICE NAME AND ADDRESS
Defense Nuclear Agency
Washington, DC 20305

12. REPORT DATE
July 1978
13. NUMBER OF PAGES
38

14. MONITORING AGENCY NAME & ADDRESS (if different from Controlling Office)
(12) 38p.

15. SECURITY CLASS. (of this report)
UNCLASSIFIED
15a. DECLASSIFICATION/DOWNGRADING SCHEDULE

16. DISTRIBUTION STATEMENT (of this Report)
Approved for public release; distribution unlimited.
(16) G37IAXY (17) X970

17. DISTRIBUTION STATEMENT (of the abstract entered in Block 20, if different from Report)

18. SUPPLEMENTARY NOTES
HDL Project: 201724
DRCMS Code: 36AA.7100.62710
This project was performed under "DNA AURORA Operations," DNA subtask G37IAXYX970, work unit 07.

19. KEY WORDS (Continue on reverse side if necessary and identify by block number)
Intense relativistic electron beams
Pinched beams

20. ABSTRACT (Continue on reverse side if necessary and identify by block number)
The AURORA pulser, which normally operates as a pulsed bremsstrahlung machine, has been modified to inject the electron beam from one of the four lines into a drift chamber. The beam obtained from a hemispheric cathode and a machine charging voltage of 90 kV has been studied in detail. This beam of 8 MeV, 240 kA, 200 ns, 300 kJ has produced energy fluences of 10 to 500 cal/cm^2. sq. cm.
The energy deposition profile in three materials has been measured and calculated with reasonable agreement. The beam has been

next page

DD FORM 1 JAN 73 1473 EDITION OF 1 NOV 65 IS OBSOLETE 1 UNCLASSIFIED
SECURITY CLASSIFICATION OF THIS PAGE (When Data Entered)

successfully used for structures testing, fluidics circuit irradiation, high intensity bremsstrahlung production, and collective ion acceleration.

LEVEL II

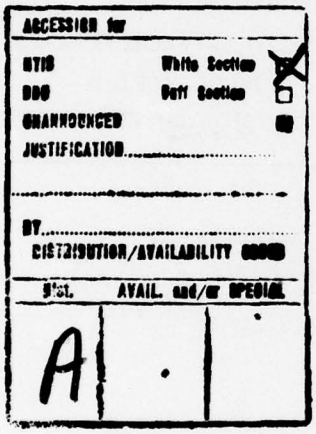

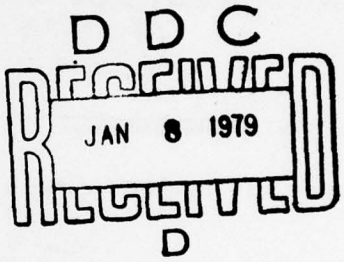

CONTENTS

FIGURES

CONTENTS (Cont'd)

1. INTRODUCTION

The AURORA Facility is sponsored by the Defense Nuclear Agency (DNA) and operated by the Harry Diamond Laboratories (HDL) to simulate nuclear-weapon gamma-ray induced radiation effects. The facility has been operational since April 1972. The output of the simulator in the bremsstrahlung mode is described in the AURORA Facility User's Brochure.

The simulator is the largest of a class of machines known as flash x rays. All of these machines involve the slow charge (microseconds to seconds) of a pulse-forming line and the production of a fast pulse (10 to 100 ns) by the discharge of the line. The AURORA simulator uses a 12-MV, 5-MJ Marx generator to charge four triaxial pulse-forming lines (Blumleins). The theory and the operation of the pulser have been described in detail by the designers.[1] In the normal bremsstrahlung mode, each of the four diodes delivers an electron beam of 10 MeV, 290 kA, 200 ns onto a tantalum target using 110 kV charging voltage on the Marx generator. This condition amounts to 2.9 MJ total energy delivered.

The conversion from the flash x-ray mode to the pulsed beam mode consists essentially of replacing the bremsstrahlung target with a thin window and allowing the beam to pass from the acceleration region into a drift region where the beam's behavior is controlled by its own electric and magnetic fields.

A review[2] of previous beam studies contains a list of references through 1971. These studies cover the work that is pertinent to this report. Reference to more recent works can be found in books by Davidson[3] and by Lawson.[4] A sketch of the theory of beam propagation is given in section 2 of this report, and a more rigorous treatment is given by Davidson[3] and by Lawson.[4]

The electron beam conversion of the AURORA pulser was undertaken by the AURORA staff less than 1 year after the facility was opened to users. In April 1973, the first beam experiments were conducted. These experiments have continued under funding by DNA in the following fields:

- Structures and materials heating
- Pinched beam, high intensity bremsstrahlung production
- Collective ion acceleration

---

[1] *B. Bernstein and I. Smith, IEEE Trans. Nucl. Sci., NS-20 (1973), 294.*

[2] *S. E. Graybill, IEEE Trans. Nucl. Sci., NS-18 (1971), 438.*

[3] *Ronald C. Davidson, Theory of Nonneutral Plasmas, W. A. Benjamin, Inc., Reading, MA (1974).*

[4] *J. D. Lawson, The Physics of Charged Particle Beams, Clarendon Press, Oxford (1977).*

This report deals mainly with the beam parameters useful to the materials and structures response experimenters.

2. THEORY

Figure 1 depicts the basic forces acting on a beam. The electrons are accelerated from the cathode to the anode, which is thin compared to the range of the electrons. (The cathodes in these pulsed high voltage machines are field-emission initiated plasma sources, which result in a space-charge-limited electron flow.) The electrons pass through the window into the drift region, where the only fields present are from the beam itself. The beam's circumferential magnetic field produces a compressive force on the beam, and the radial electric field produces a divergent force on the beam. Magnetic interaction of the beam with the wall return current stabilizes the beam toward the center of the drift tube. The plasma return current reduces the net current in the drift chamber and therefore reduces the magnetic field.

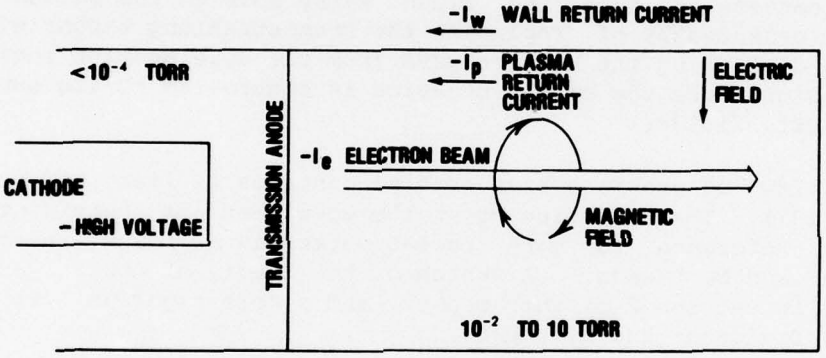

Figure 1. Fields and currents of drifting electron beam.

Assuming a beam long compared to its diameter and of uniform current density, the repulsive coulomb force and the magnetic compressive force are

$$eE_r = \left[\frac{e}{\beta}\frac{1}{2\pi}\left(\frac{\mu}{\epsilon}\right)^{\frac{1}{2}}(1 - f)\right]\begin{cases}\dfrac{Ir}{r_b^2}, & 0 < r \le r_b, \\ \dfrac{I}{r}, & r_b \le r < \infty,\end{cases}$$

and

$$ev_z B_\theta = \left[e\beta\frac{1}{2\pi}\left(\frac{\mu}{\epsilon}\right)^{\frac{1}{2}}\right]\begin{cases}\frac{Ir}{r_b^2} & , \quad 0 < r \leq r_b \quad , \\ \frac{I}{r} & , \quad r_b \leq r < \infty \quad ,\end{cases}$$

where

e = charge of electron in coulombs,

E_r = radial electric field in volts per meter,

β = v/c,

β_r = v_r/c,

β_z = v_z/c,

v = electron velocity in meters per second,

v_r = radial velocity,

v_z = longitudinal velocity,

c = velocity of light in vacuum in meters per second,

μ = permeability of free space in henries per meter,

ϵ = permittivity of free space in farads per meter,

f = ratio of plasma ion to beam electron density,

I = net current in amperes,

r = radial distance in meters,

r_b = beam radius in meters,

B_θ = circumferential magnetic field in tesla.

The net inward force in the beam is

$$eE_r(\text{net}) = ev_z B_\theta - eE_r = \frac{e}{\beta}\frac{1}{2\pi}\left(\frac{\mu}{\epsilon}\right)^{\frac{1}{2}}\frac{Ir}{r_b^2}\left(\beta^2 - 1 + f\right) \quad , \quad 0 < r \leq r_b .$$

Therefore, the beam will be magnetically self-confined if the ionization fraction $f > 1 - \beta^2 = 1/\gamma^2$, where $\gamma = (eV/mc^2) + 1$. A 1-MeV beam needs about a 10-percent ion-to-electron ratio and a 10-MeV beam needs about a 0.25-percent ratio to satisfy this condition.

The first calculations of the behavior of self-pinched beams were done by Bennett,[5] followed by a very useful analysis by Lawson.[6] Lawson's analysis contains many simplifying assumptions. He assumes uniform current density, charge neutralization, a beam long compared to its radius, and most importantly he assumes small radial motion, or $\beta_r << \beta_z$ = constant. This is the paraxial approximation, which permits one to perform a simple calculation of the particle trajectories. Assuming charge neutralization and remoteness from the beam front implies that the electrons have a constant γ since there are no potential gradients.

With these assumptions, we can write a simple radial equation of motion,

$$\gamma m\ddot{r} = -e\beta_z cB_\theta = \frac{-e\beta_z c\mu I}{2\pi r_b^2} r \quad , \quad 0 \le r \le r_b \quad ,$$

where m = mass of electrons in kilograms.

Having assumed $\beta_z = \beta$ = constant, then $\dot{r} = (dr/dz)(dz/dt) = (dr/dz)\beta c$ and $\ddot{r} = \beta^2 c^2 (d^2r/dz^2)$, so

$$\frac{d^2r}{dz^2} + \frac{e\mu I}{2\pi r_b^2 m\beta\gamma c} r = 0 \quad .$$

Lawson defined the dimensionless parameter ν/γ, where ν is the number of electrons per classical electron radius measured longitudinally along the beam. The number per unit length is given by $N_e = I/e\beta c$, and the classical electron radius is given by $r_e = e^2/4\pi\varepsilon mc^2$.

---

[5] *W. H. Bennett, Phys. Rev., 45 (1934), 890; 98 (1955), 1584.*

[6] *J. D. Lawson, J. Electronics and Controls, 3 (1957), 587; 5 (1958), 146.*

$$\nu = N_e r_e$$

and

$$\frac{\nu}{\gamma} = \frac{Ie}{\beta\gamma 4\pi\varepsilon mc^3} = \frac{Ie\mu}{\beta\gamma 4\pi mc} \quad \left(\text{using } c^2 = \frac{1}{\mu\varepsilon}\right) .$$

Then,

$$\frac{d^2r}{dz^2} + \frac{2\nu}{\gamma}\frac{r}{r_b^2} = 0$$

The solution is sinusoidal with wavelength λ, where

$$\lambda = \frac{2\pi r_b}{\left(2\frac{\nu}{\gamma}\right)^{\frac{1}{2}}} .$$

For the paraxial approximation to hold, $\lambda > 2\pi r_b$, and therefore $\nu/\gamma < 1/2$ is required. (This follows from requiring $|dr/dz| < 1$.)

Evaluating the constants,

$$\frac{\nu}{\gamma} = \frac{I}{17{,}000\beta\gamma} .$$

ν/γ is inversely related to the gap impedance. Since

$$\beta\gamma = \left(\gamma^2 - 1\right)^{\frac{1}{2}} \quad .$$

and

$$V = \frac{mc^2}{e}\,(\gamma - 1) \quad ,$$

$$\frac{\nu}{\gamma} = \frac{I}{\left(\gamma^2 - 1\right)^{\frac{1}{2}}}\,\frac{30(\gamma - 1)}{V} = \frac{30}{Z_b}\left(\frac{\gamma - 1}{\gamma + 1}\right)^{\frac{1}{2}} \quad ; \quad \text{for} \quad \gamma >> 1, \quad \frac{\nu}{\gamma} \approx \frac{30}{Z_b} \quad ,$$

where $Z_b = V/I$ is the gap impedance.

One can also derive the ν/γ limit by considering the Larmor radius, ρ_L, of an electron at the edge of the beam:

$$\rho_L = \frac{p}{eB} = \frac{m\gamma\beta c}{e}\,\frac{2\pi r_b}{\mu I} \quad ,$$

where p is the electron momentum.

Then $r_b/\rho_L = 2\nu/\gamma$, so when $\nu/\gamma = 1/2$, the Larmor radius is equal to the beam radius, and the beam would not be expected to propagate efficiently.

The behavior of electron beams as predicted by the preceding calculations has been well verified.[2] It has been experimentally observed that beams achieve force neutralization and become self-focusing at about 0.1 Torr of background gas. This pressure of 0.1 Torr is slightly higher than one would calculate with the relationships just presented, due to the effect of beam divergence and scatter on entrance into the drift chamber. Minimum net current, that is, when most of the return current is carried in the plasma, is always observed at about 1 Torr of pressure. Beams propagate most efficiently at minimum net current and propagate *only* if $I_{net}/17{,}000\beta\gamma < 1$.[7] For beams of $\nu/\gamma > 1$, one needs an external magnetic field to keep the beam from collapsing. Extremely high ν/γ beams such as those from each of

---

[2] *S. E. Graybill, IEEE Trans. Nucl. Sci., NS-18 (1971), 438.*

[7] *P. Spence and G. Yonas, Record of the 10th Symposium on Electron, Ion and Laser Beam Technology, L. Marton, Ed., IEEE Catalog No. 69C22-Ed (1969), 443.*

the CASINO diodes (at the Naval Surface Weapons Center), where $\nu/\gamma = 20$, utilize both plasma return currents to minimize I_{net} and applied magnetic fields of about 20 kg. The AURORA beam studies have all been at $\nu/\gamma \approx 1$.

3. BEAM CONVERSION

To maximize the bremsstrahlung field, the termination of the vacuum coaxial lines which form the bremsstrahlung targets is not cylindrically symmetric.[1] In figures 2 and 3, a bremsstrahlung anode tip is shown on the upper left of the four vacuum coaxial lines. The first beam conversion consisted of extending this upper left coaxial line. This extension required removing the other three anode tips, grounding the other three tubes, and installing dummy loads on those Blumleins. These early beam experiments were successful, but the turnaround time from the bremsstrahlung to beam operation was almost 1 week.

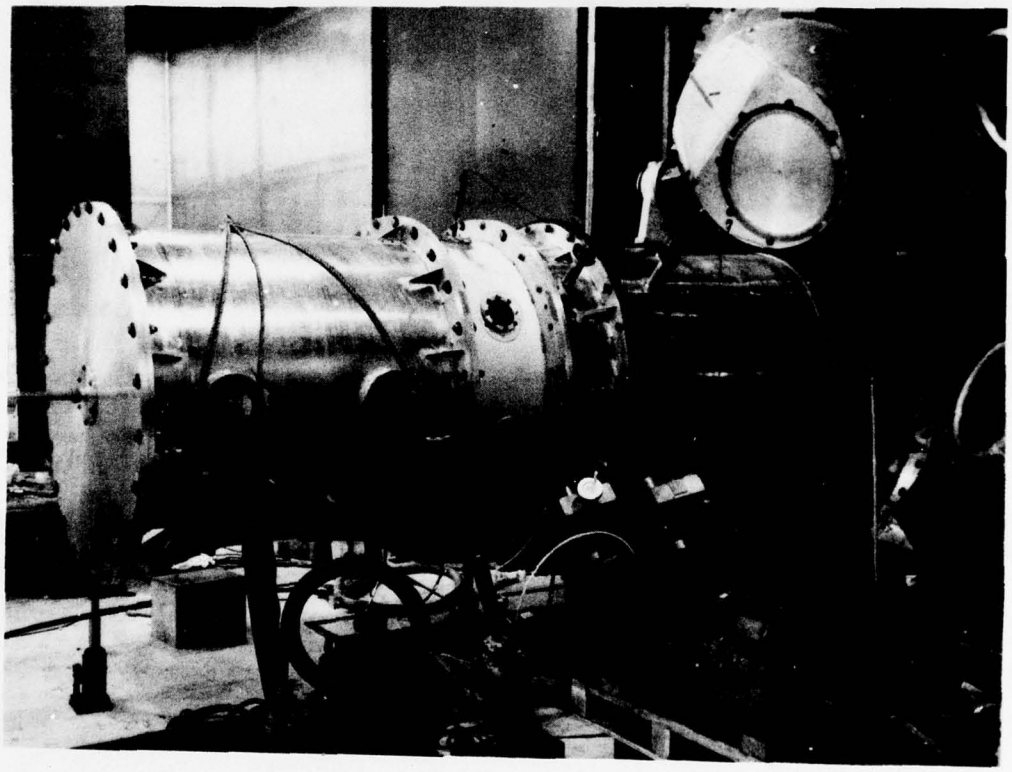

728-74(1)

Figure 2. AURORA electron beam hardware.

[1] *B. Bernstein and I. Smith, IEEE Trans. Nucl. Sci., NS-20 (1973), 294.*

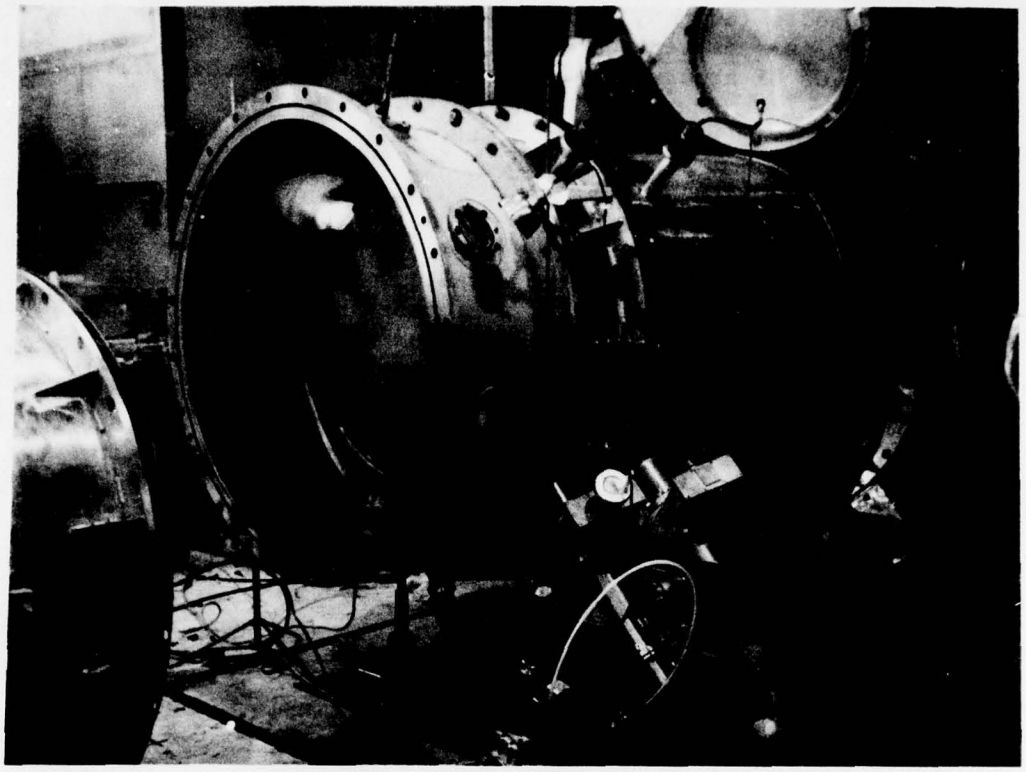

728-74(2)

Figure 3. AURORA electron beam hardware showing titanium beam window.

To shorten the conversion time and to operate in the horizontal world, the equipment shown in figures 2 and 3 was built to fit on the lower left coaxial line. This method allows the beam to be operated without any change in the other three lines, which pulse in the normal bremsstrahlung mode. This conversion can be and has been done in 1 day. A 45-deg bend is placed in the vacuum coaxial line, followed by the window anode shown in figure 3 at the end of a straight section. The vacuum coaxial line is a 50-Ω structure with a 1.22-m-diameter outer conductor and a 0.53-m-diameter inner conductor. These dimensions were continued into the beam equipment. The transmission window is 0.91 m in diameter and is 0.04-cm-thick titanium. The drift chamber is 1.22 m in diameter and 1.22 m long.

The vacuum coaxial lines require magnetic insulation to work properly.[1] It is shown in appendix A that it is necessary for

$$Z_{gap} < Z_0\left(\frac{\gamma - 1}{\gamma + 1}\right)^{\frac{1}{2}}$$

[1] *B. Bernstein and I. Smith, IEEE Trans. Nucl. Sci., NS-20 (1973), 294.*

where Z_0 is the characteristic impedance of the coaxial line, for radially emitted electrons from the inner conductor of the coaxial line to be trapped inside the outer conductor and be swept downstream. If this magnetic insulation is not present, the entire current output of the pulser can be shunted off through field emission in the coaxial lines. The 45-deg bend in the coaxial line reduces the magnetic field by about 30 percent and puts severe limits on the gap impedance.

It is shown in the appendix that the turnaround distance, r, of a radially emitted electron is given by

$$\ln \frac{r}{r_i} = \frac{17{,}000}{I} \frac{\frac{Z_b}{Z_0}}{1 - \left(\frac{Z_b}{Z_0}\right)^2}$$

where r_i is the radius of the inner conductor and Z_0 is the characteristic impedance of the line. Figure 4(a) shows the turnaround radius as a function of beam impedance for the case of the 50-Ω coaxial line and various beam currents. Figure 4(b) shows the same calculation where the magnetic field is reduced by 27 percent by the 45-deg bend.

The results to date with the bent coaxial line indicate that there is some loss from emission in the line when the anode-cathode gap is about 30 Ω. Attempts to produce lower impedance gaps have failed, possibly because the cathode "turn on" time (the time required to form the cathode plasma) is long enough for the emission in the line to start in spite of the geometrical gap impedance.

The first cathode used was similar to the bremsstrahlung cathode. It was a torus with a 0.53-m major diameter and a 5-cm minor diameter. The beam produced by it did not pinch, and only low energy fluences were obtained. The next cathode used was a 0.53-m-diameter hemisphere, which produced a suitable beam. However, on many occasions there was considerable damage to the end of the cathode. It was concluded that the damage was due to the electrons flowing during the voltage reversal, which occurs 200 ns after the peak of the main pulse. This reversal is about 1 MeV and 100 kA, according to the pulser diagnostics and, occurring this late in time, is probably a well-pinched beam due to ions in the gap. The first solution to this problem was to use carbon and steel caps on the aluminum hemisphere, but the best results were obtained by the present hemisphere with a 15.2-cm hole on center surrounded by a rollup. All the data in this report are from this cathode at a spacing of 23 cm.

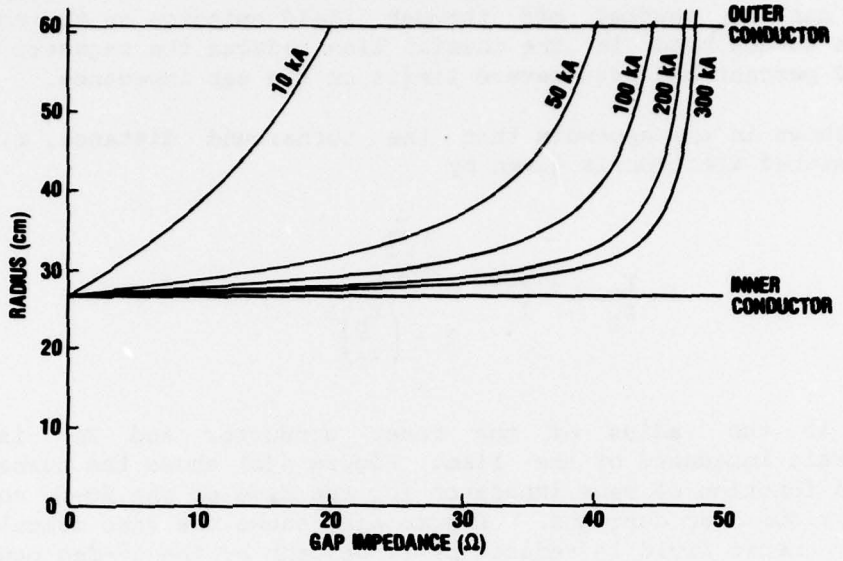

(a)

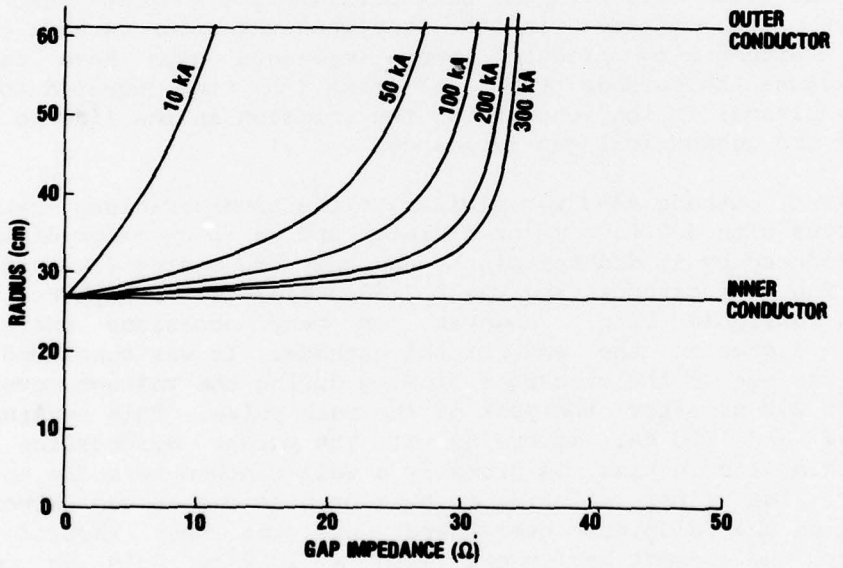

(b)

Figure 4. Electron turning point in 50-Ω vacuum coaxial line for various currents as function of gap impedance: (a) straight coaxial line and (b) 45-deg bend in coaxial line.

The relative entrance current density was measured with the blue cellophane dosimetry system.[8] This blue cellophane (Dupont MSC-300) is a dosimeter that increases in its transmission of light at the transmission minimum (approximately 650 nm) in proportion to the absorbed dose. The cellophane reader uses a helium-neon laser at 632.8 nm, which is sufficiently close to the transmission minimum. Since the cellophane is a thin (3.5 mg/cm^2) dosimeter and the beam electrons are in the MeV range, where the stopping power is only weakly dependent on energy, the dose is proportional to the incident charge density and is given by

$$D = \frac{1}{\rho}\frac{dE}{dx}\phi_e$$

where

D is the dose in J/g,

$(1/\rho)(dE/dx)$ is the stopping power in MeV-cm^2/g,

ϕ_e is the electron fluence in $\mu C/cm^2$.

Since 1 Mrad is equal to 10 J/g and, for carbon,

$$\frac{1}{\rho}\frac{dE}{dx} \simeq 2\ \frac{\text{MeV-cm}^2}{\text{g}}$$

then 5 $\mu C/cm^2$ produces about 1 Mrad in the cellophane.

Figure 5 shows the change in transmission of the cellophane as a function of radius at the beam entrance window. These data are from two shots which were superimposed on the same cellophane to raise the signal. The sensitivity of the system, stated by the manufacturer, is D (Mrad) = $(1/2)\Delta T$, where ΔT is the increase in transmission. The calculated charge density integrated over $2\pi r\, dr$ then yields a total charge of 4.4×10^{-2} C. Since the pulse width is 200 ns, we calculate a current of ≈220 kA, which is in reasonable agreement with the pulser diagnostics.

---

[8] *SPI-Rad Thin Film Dosimetric System, Simulation Physics Inc., Burlington, MA [n.d.].*

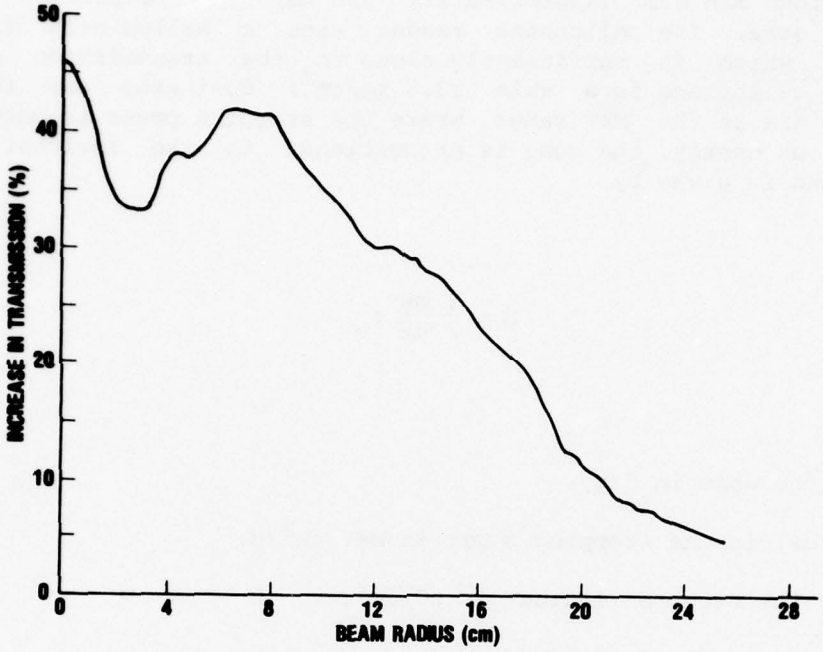

Figure 5. Current density at beam window measured with blue cellophane: 0.53-m-diameter hemispherical cathode and 0.23-m anode-cathode gap.

Figure 6 shows the normalized integrated current as a function of r,

$$\frac{I(r)}{I} = \frac{\int_0^r j2\pi r\, dr}{\int_0^{r_b} j2\pi r\, dr}$$

where r_b is the radius of the beam; most of the current is inside a 0.48-m-diameter circle.

The voltage and the current are determined by the pulser diagnostics operated and calibrated by the AURORA Operation and Maintenance Group and have been corroborated by depth dose measurements (sect. 5). Representative voltage and current waveforms are shown in figure 7.

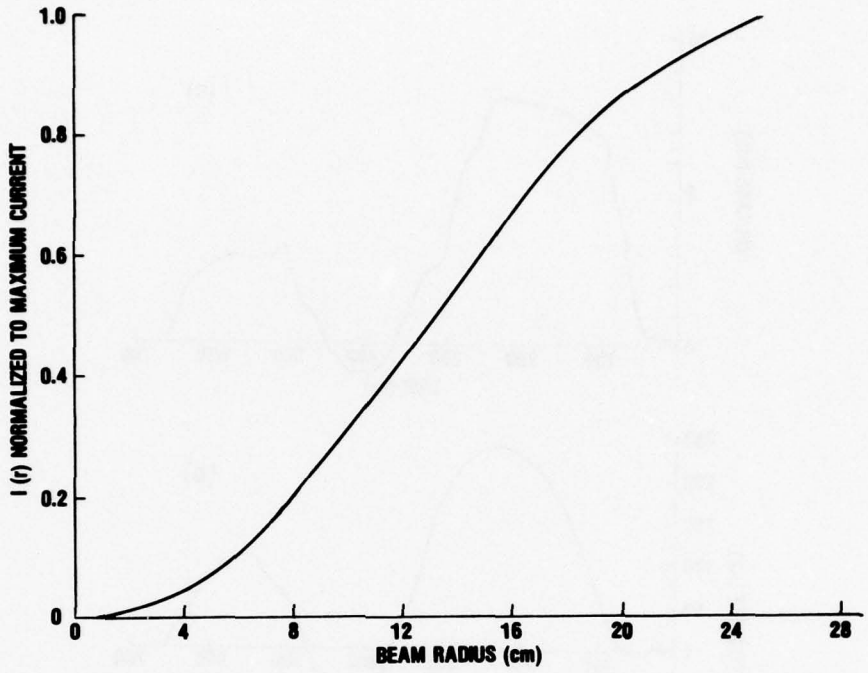

Figure 6. Integrated electron beam current density as function of radius, normalized to total current: 0.53-m-diameter cathode and 0.23-m anode-cathode gap.

The voltage monitor is a capacitive sensor on the inside surface of the outer element of the vacuum coaxial line. (This monitor was designed and constructed by AURORA personnel.) The current monitor is a 7-mΩ belt of carbon resistors that interrupts the return current in this outer element of the coaxial line. These monitors are of the same type as used on the HDL HIFX Facility.[9] The voltage pulse has been corrected for the capacitive discharge that takes place during the pulse. It is easy to show that

$$V(t) = V_0(t) + \frac{1}{RC} \int_0^t V_0(t)\, dt \quad ,$$

where V(t) is the corrected voltage pulse from the monitor, $V_0(t)$ is the observed pulse, and RC is the time constant of the monitor. In the case of the monitor used here, the RC time is 2600 ns.

[9] *F. J. Sazama and A. G. Stewart, Design and Testing of a Current and Voltage Monitor for HIFX, Harry Diamond Laboratories TR-1558 (1971).*

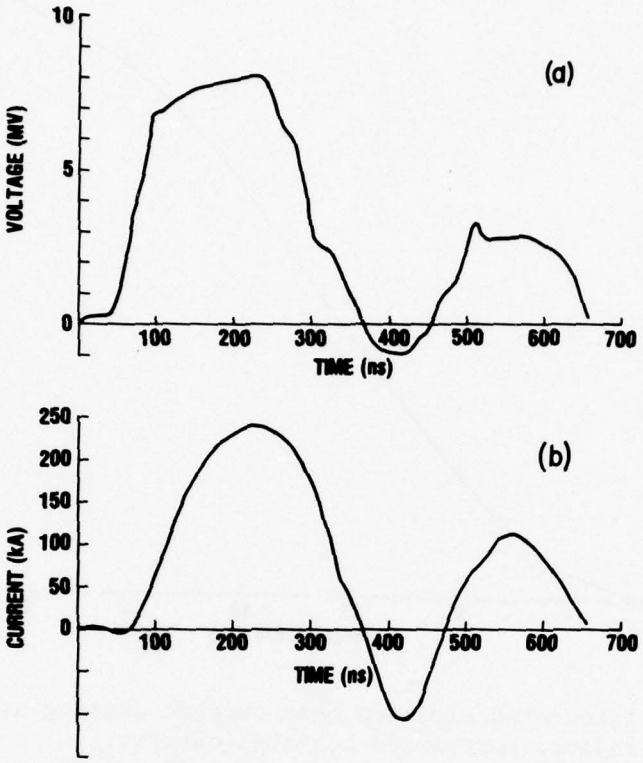

Figure 7. AURORA diode voltage and current at 90-kV charging voltage: (a) cathode voltage as function of time and (b) cathode current as function of time.

The voltage and current traces are digitized by using the Hewlett-Packard 9820A programmable calculator, which also interpolates values at equal time increments and corrects the voltage trace for the capacitive slump. The equal time interval current and voltage data are entered in a program called EBSPEC,[10] which calculates an electron spectrum. The use of these spectra is discussed in section 5. Table I summarizes the beam parameters.

The 110-kV charging voltage is the normal maximum operating level, but 90 kV was used for almost all of the beam shots to extend the period between machine failures. The 90-kV charging voltage beam was used for all of the data reported in the following sections, except where otherwise noted.

---

[10] *A Technical Report: Program EBSPEC, Simulation Physics Inc. Technical Report TR-71-06 (1971).*

TABLE I. ELECTRON BEAM PARAMETERS

Parameter	Charging voltage	
	90 kV	110 kV
Max electron energy	8 MeV	10 MeV
Max beam current	240 kA	290 kA
Total beam energy	290 kJ (primary pulse) + 30 kJ in first reflection	480 kJ
Pulse width	200 ns FWHM	200 ns FWHM
Av electron energy	5.6 MeV	7 MeV

4. ENERGY FLUENCE MEASUREMENTS

The materials response experimenter must know the energy fluence and the energy depth deposition to calculate the response of the materials. The beam must be reproducible since the only type of diagnostics that can be used on a sample exposure is a thin foil calorimeter.

The energy fluence is normally measured with a total stopping calorimeter. The beam energy is absorbed, usually in carbon, and the temperature rise of the absorber is measured. Figure 8 shows the segmented carbon calorimeter manufactured by Simulation Physics Inc. (SPI) and used at AURORA. There are 53 absorbers, each a 3.8-cm-thick piece of carbon with a Chromel-Alumel thermocouple attached to the rear. The "cold" junction is at room temperature and occurs where the thermocouple leads are connected to feed-through connectors. The contiguous absorbers cover an 18-cm-diameter circle, with the four 2.5-cm-diameter outer probes centered on a 26-cm-diameter circle. Each thermocouple junction voltage is carried to the data room on a twisted shielded pair cable which passes through relays (which are opened at shot time) and through low pass filters. The voltage is read out with 5-μV precision on a Vidar data scanner. The carbon absorbers take several seconds to come to their equilibrium temperature and have a thermal decay time of several minutes so that the calorimeters can be isolated from the Vidar unit at shot time with the relays and connected immediately after the shot; thus, the high voltage transients are isolated from the data scanner.

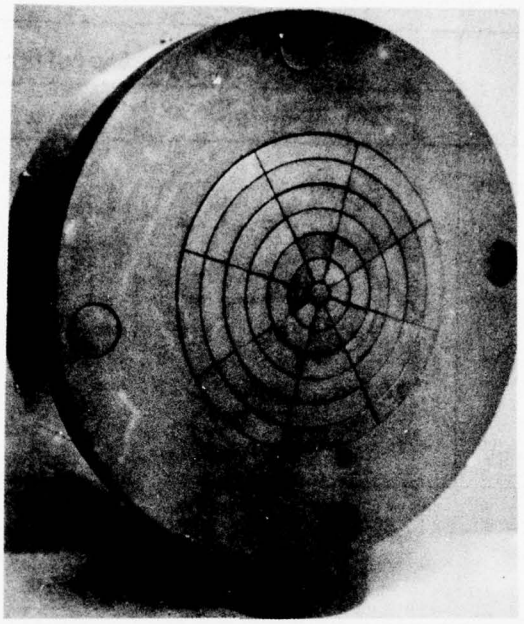

Figure 8. Graphite beam mapping calorimeter head.

The calibration of the absorbers has been supplied by SPI and includes the variation of the specific heat of carbon with temperature and the nonlinearity of the thermocouple output. The calibration curve has been fitted with a cubic equation, and the data are reduced on the Hewlett-Packard 9820A.

Figure 9 shows the fluence versus the radius for two beam drift distances. The 10-cm drift distance produces the maximum fluence obtained from this beam. (The first, 45-deg, beam chamber produced fluences about 30 percent higher.) The 25-cm drift distance produces a lower, more uniform fluence. These radial plots are obtained by averaging the fluence seen in the eight segments of each ring; this averaging is valid if the beam is reasonably symmetric. Figure 10 shows the isofluence contours for shot 2069, which are nearly cylindrically symmetric.

The integrated energy over the entire calorimeter array for shot 2069 is 187 kJ, or about 60 percent of the total beam energy. The remaining 40 percent of the energy falls outside the calorimeter and, in most cases, is wasted. This loss is the price of using a self-focused beam, as opposed to using external magnetic guide fields.

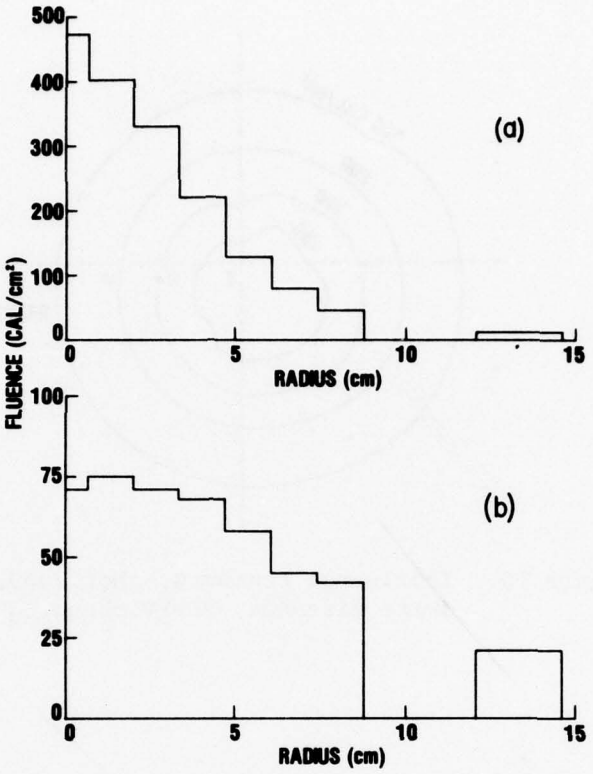

Figure 9. Energy fluence versus radius (90-kV charging voltage): (a) shot 2069, 10-cm drift distance, and (b) shot 1891, 25-cm drift distance.

It is clear from these fluence versus radius plots that there is a trade-off to be made between fluence and area for a given uniformity. At 45-cm drift distance, the fluence is down to about 20 cal/cm^2, but is almost uniform across the calorimeter. Plots of fluence versus drift distance and of beam radius versus drift distance are shown in figure 11.

In the original beam setup (45-deg chamber), a study was made of the beam reproducibility; the fluence calorimeter showed no worse than a 13-percent rms scatter on any single channel for eight shots. This is a severe test since it takes both beam wander and machine variation into account.

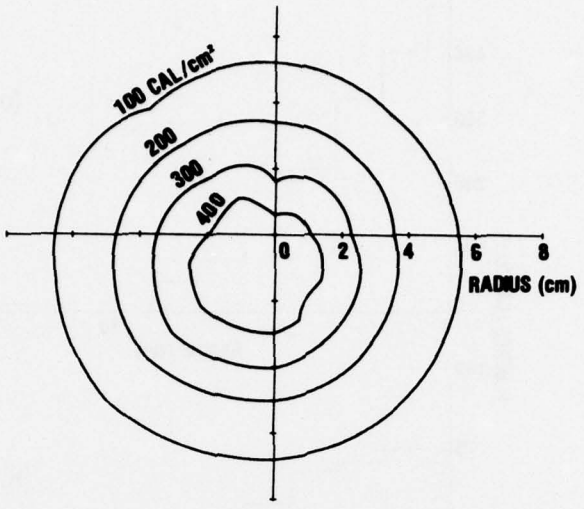

Figure 10. Isofluence contours, shot 2069, 10-cm beam drift distance, 90-kV charging voltage.

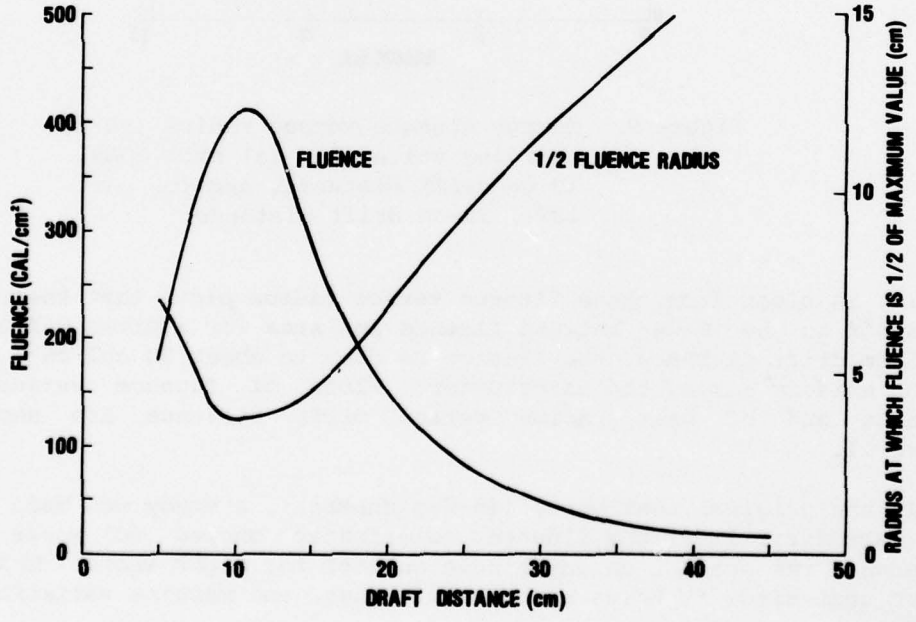

Figure 11. Energy fluence versus drift distance at 1-Torr pressure (air) and radius at which fluence is one half of maximum value versus drift distance.

5. ENERGY DEPOSITION

The material response experimenter must know, in addition to the energy fluence already discussed, the energy depth deposition profile. If one knows the electron energy spectrum, the depth dose is, in principle, calculable. This section describes the comparison of such calculations with experimental results.

The electron spectrum was derived from the current and voltage profiles in figure 8 and is shown in figure 12(a). The voltage and the current are digitized for input into the computer code EBSPEC,[10] which calculates the electron spectrum, among other results. The low energy peak between 2.5 and 3.5 MeV is a result of the reflection seen in the current and voltage pulses. The average electron energy in the spectrum is 5.6 MeV.

The effect of the 0.04-cm-thick titanium window was calculated by using the above spectrum as input into the Monte Carlo transport program EZTRAN.[11] The calculated spectrum of the electrons emerging from the titanium window is shown in figure 12(b). The average electron energy is reduced to 5.3 MeV. This average energy loss of 300 keV agrees with that calculated by using the window thickness and dE/dx for relativistic electrons.

Finally, this spectrum is used as input into EZTRAN to calculate the deposition profile in a given material. EZTRAN can handle alloys by averaging the atomic numbers weighted by their fraction of the total weight, but cannot treat laminates. Deposition calculations have been done for aluminum, iron, and tantalum; the results are shown in figure 13. (A new transport program named "TIGER" is in use and can treat laminates of different materials.)

The experimental points were measured by using the blue cellophane already discussed in section 3. The cellophane dosimeters are sandwiched between absorbers, and several shots were superimposed for each measurement. Also, single shot calorimeter measurements were performed and were in substantive agreement with the blue cellophane measurements. The cellophane has one great advantage over calorimeters in that the absorbers do not have to be separated to avoid thermal cross talk so that the experiment comes nearer to the assumption of the EZTRAN calculation of a uniform homogeneous absorber. The experimental points

---

[10] *A Technical Report: Program EBSPEC, Simulation Physics Inc. Technical Report TR-71-06 (1971).*

[11] *J. A. Halbleib, Sr., and W. H. Vandevender, EZTRAN--A User-Oriented Version of the ETRAN 15 Electron-Photon Monte Carlo Technique, Sandia Laboratories, Albuquerque, NM, Report SC-DR-71 0598 (September 1971).*

are shown in figure 13; the agreement with EZTRAN is good for aluminum and iron. In tantalum, the extrapolated ranges of theory and experiment agree, but the calculated front surface dose is larger than that measured. This discrepancy is not understood at this time.

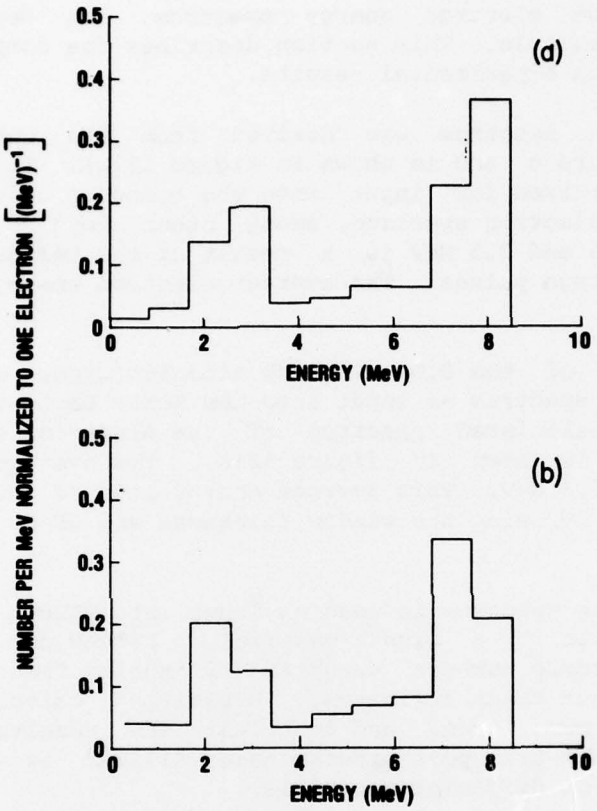

Figure 12. Electron energy spectrum (90-kV charging voltage): (a) initial spectrum, calculated from current and voltage profiles, $\overline{ev}$ = 5.6 MeV, and (b) spectrum after passing through 0.04-cm-thick titanium window--initial spectrum used as input to EZTRAN code, $\overline{ev}$ = 5.3 MeV.

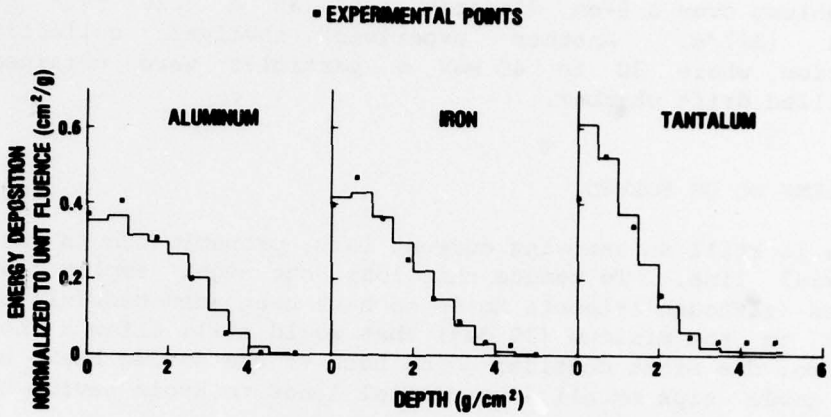

Figure 13. AURORA electron beam measured energy deposition compared with transport calculation (90-kV charging voltage).

6. BEAM APPLICATIONS

The prime reason for the development of this beam was materials and structures heating. Electrons provide the only way to get large, pulsed doses up to several hundred megarads in the laboratory, albeit with some disadvantages. The main drawback is that the deposition profile is usually not what the experimenter desires. Also, the deposition profile is not known at high fluences, nor can it be accurately calculated. The spectrum is typically obtained from current and voltage data and sometimes measured at low fluence levels. The deposition profile is necessarily measured at low fluence levels. But high fluences occur at the beam pinches where angles of incidence are unknown and dB/dt effects may influence the spectrum.

Two interesting applications have been made of the AURORA beam by other personnel of HDL. In one application, an aluminum cylinder was covered with lead to provide a large front surface impulse from the lead blowoff at the same time that the aluminum was heated in depth. In another application, a fluidic circuit was exposed to a low fluence. For this application, the beam was brought out through a second window into the test cell, so the sample could be worked on without letting the tube and the drift chamber up to air.

Other experiments, not in the materials area, have been done by AURORA personnel and will be reported separately. One of these was a study of the bremsstrahlung from a tungsten carbide target placed at the beam pinch (10-cm drift distance). We observed 200 krads (Si) of bremsstrahlung over a 5-cm diameter spot at a dose rate over 2×10^{12} rads (Si)/s. Another experiment involved collective ion acceleration, where 30 to 40 MeV α particles were obtained from a helium-filled drift chamber.

7. PROBLEMS TO BE SOLVED

There is still an annoying current loss, probably due to the bend in the coaxial line. To reduce this loss, one might employ lower gap impedances (although attempts to do so have been unsuccessful) or reduce the bend to the minimum (30 deg) that would still allow a horizontal beam. Also, one might consider going back to the 45-deg beam, but with tapered anode tips on all four coaxial lines to avoid having to ground tubes and install dummy loads.

Also, we should consider an external magnetic guide field. The problem is that, for the 2 to 4 tesla needed over a cubic meter, several megajoules of magnetic field is needed. The expense of forming this field by the conventional capacitor method is huge, but recent work on homopolar generators[12] might make this feasible.

8. SUMMARY

The AURORA pulser has been modified to produce an electron beam of 8 MeV, 240 kA, 200 ns, 300 kJ in a drift chamber. Fluences of 500 cal/cm^2 down to tens of cal/cm^2 have been produced. The energy deposition in aluminum is a maximum of 0.5 cal/g/cal/cm^2 at about 1-g/cm^2 depth. The beam has been successfully used for structures testing, fluidic circuit irradiation, high intensity bremsstrahlung production, and collective ion acceleration. The beam is reproducible from one setup to another.

---

[12] *M. Driga, S. Nasar, H. Rylander, W. Weldon, and H. Woodson, IEEE Trans. Plasma Sci., PS-3, No. 4 (1975).*

ACKNOWLEDGEMENTS

The voltage and current data along with help in interpretation were provided by Alexander Stewart and George Huttlin. Claude Rowe and Clifford Haynes played the major role in the assembly of the experimental apparatus, supplied ingenious solutions to the inevitable problems, and suggested design improvements. The performance of experiments and the data reduction and analysis were greatly facilitated by the contributions of Anahid Yeremian. The hardware designs were done by Grover Sherlin.

LITERATURE CITED

(1) B. Bernstein and I. Smith, IEEE Trans. Nucl. Sci., NS-20 (1973), 294.

(2) S. E. Graybill, IEEE Trans. Nucl. Sci., NS-18 (1971), 438.

(3) Ronald C. Davidson, Theory of Nonneutral Plasmas, W. A. Benjamin, Inc., Reading, MA (1974).

(4) J. D. Lawson, The Physics of Charged Particle Beams, Clarendon Press, Oxford (1977).

(5) W. H. Bennett, Phys. Rev., 45 (1934), 890; 98 (1955), 1584.

(6) J. D. Lawson, J. Electronics and Controls, 3 (1957), 587; 5 (1958), 146.

(7) P. Spence and G. Yonas, Record of the 10th Symposium on Electron, Ion and Laser Beam Technology, L. Marton, Ed., IEEE Catalog No. 69C22-Ed (1969), 443.

(8) SPI-Rad Thin Film Dosimetric System, Simulation Physics Inc., Burlington, MA [n.d.].

(9) F. J. Sazama and A. G. Stewart, Design and Testing of a Current and Voltage Monitor for HIFX, Harry Diamond Laboratories TR-1558 (1971).

(10) A Technical Report: Program EBSPEC, Simulation Physics Inc. Technical Report TR-71-06 (1971).

(11) J. A. Halbleib, Sr., and W. H. Vandevender, EZTRAN--A User-Oriented Version of the ETRAN 15 Electron-Photon Monte Carlo Technique, Sandia Laboratories, Albuquerque, NM, Report SC-DR-71 0598 (September 1971).

(12) M. Driga, S. Nasar, H. Rylander, W. Weldon, and H. Woodson, IEEE Trans. Plasma Sci., PS-3, No. 4 (1975).

APPENDIX A.--MAGNETIC INSULATION

In the design of the AURORA pulser, Physics International Co. (PI) recognized that, to bring the power from the four Blumleins to four closely spaced targets, they would need longer cathode stalks than had been necessary in previous smaller machines. These stalks, which together with their outer conductors are known as the "vacuum coaxes," are long enough to be treated as transmission lines. Further, PI realized that the current loss due to field emission from the large area of the vacuum coax could be catastrophic. Although field emission currents at these field strengths are less than 1 A/cm^2, the areas of the vacuum coaxes are over 2×10^5 cm^2 each. Therefore, only if the field emission current from the inner coax element is magnetically suppressed can the large area coax idea work.

Assuming cylindrical symmetry, we calculate the conditions under which an electron emitted from the inner coax surface at radius r_i is turned back by the magnetic field before hitting the outer wall at radius r_o. In this single particle model, the electron is bent downstream and back to the inner coax element, where the process is repeated so that there is a net downstream motion of the field emitted electrons.

The magnetic field is

$$B_\theta = \frac{\mu I}{2\pi r} \quad ,$$

where I is the cathode current and μ is the permeability of free space.

The electric field is

$$E_r = \frac{V_c}{r \ln \frac{r_o}{r_i}} \quad ,$$

where V_c is the cathode voltage, and the electron energy is

$$e\left(V_c - V\right) = e\int_{r_i}^{r} E_r \, dr = \frac{eV_c \ln \frac{r}{r_i}}{\ln \frac{r_o}{r_i}} \quad .$$

APPENDIX A

The magnitude of the electron's momentum is related to its energy by

$$|p| = mc(\gamma^2 - 1)^{\frac{1}{2}} = mc\left\{\left[\frac{e(V_c - V)}{mc^2}\right]^2 + 2\frac{e(V_c - V)}{mc^2}\right\}^{\frac{1}{2}} .$$

As the electron is accelerated toward the outer coax, the B_θ field pushes it downstream with a force of $F_z = eB_\theta \, dr/dt$. The magnitude of momentum is a function only of radial position, and the magnetic field can change only the direction of the electron's momentum. The z component of momentum is given by

$$p_z = \int F_z \, dt = \int_{r_i}^{r} eB_\theta \, dr = \frac{e\mu I}{2\pi} \ln \frac{r}{r_i} .$$

The electron has been turned when $p_z = |p|$ or when

$$\frac{e\mu I}{2\pi} \ln \frac{r}{r_i} = mc\left[\left(\frac{eV_c}{mc^2} \frac{\ln \frac{r}{r_i}}{\ln \frac{r_o}{r_i}}\right)^2 + 2\frac{eV_c}{mc^2} \frac{\ln \frac{r}{r_i}}{\ln \frac{r_o}{r_i}}\right]^{\frac{1}{2}} .$$

Multiplying both sides by $(c/e)\left[(\ln r_o/r_i)/(\ln r/r_i)\right]$,

$$\frac{\mu cI}{2\pi} \ln \frac{r_o}{r_i} = \left(V_c^2 + 2\frac{mc^2}{e} V_c \frac{\ln \frac{r_o}{r_i}}{\ln \frac{r}{r_i}}\right)^{\frac{1}{2}} .$$

Since

$$\frac{\mu c}{2\pi} = \frac{1}{2\pi}\left(\frac{\mu}{\varepsilon}\right)^{\frac{1}{2}} ,$$

we recognize the transmission line characteristic impedance on the left. Denoting it as Z_0 and squaring both sides,

$$(IZ_0)^2 = V_c^2 + 2\frac{mc^2}{e} V_c \frac{\ln \frac{r_o}{r_i}}{\ln \frac{r}{r_i}} \quad .$$

Defining the beam "impedance" as $V/I = Z_b$,

$$\left(\frac{Z_0}{Z_b}\right)^2 - 1 = 2\frac{mc^2}{eV_c} \frac{\ln \frac{r_o}{r_i}}{\ln \frac{r}{r_i}} = \frac{2mc^2}{eV_c} \frac{Z_0}{\left(\ln \frac{r}{r_i}\right)\frac{1}{2\pi}\left(\frac{\mu}{\varepsilon}\right)^{\frac{1}{2}}} \quad .$$

The turning point r is then given by

$$\ln \frac{r}{r_i} = \frac{2\frac{mc^2}{eV_c} \frac{Z_0}{\frac{1}{2\pi}\left(\frac{\mu}{\varepsilon}\right)^{\frac{1}{2}}}}{\left(\frac{Z_0}{Z_b}\right)^2 - 1} \quad .$$

Once again noting that $mc^2/e = 5.11 \times 10^5$ V and $(1/2\pi)(\mu/\varepsilon)^{\frac{1}{2}} = 60\ \Omega$, we have

$$\ln \frac{r}{r_i} = \frac{\frac{17,000}{V_c} Z_0}{\left(\frac{Z_0}{Z_b}\right)^2 - 1} \quad ,$$

where r is the radius at which the electron velocity is parallel to the cylinder axis. This expression is more commonly stated with current as the independent variable:

$$V = IZ_b \quad ,$$

$$\ln \frac{r}{r_i} = \frac{17{,}000}{I} \frac{\frac{Z_0}{Z_b}}{\left(\frac{Z_0}{Z_b}\right)^2 - 1} = \frac{17{,}000}{I} \frac{\frac{Z_b}{Z_0}}{1 - \left(\frac{Z_b}{Z_0}\right)^2} \quad .$$

Going back to a previous expression,

$$\ln \frac{r}{r_i} = \frac{2\frac{mc^2}{eV_c} \ln \frac{r_o}{r_i}}{\left(\frac{Z_0}{Z_b}\right)^2 - 1} \quad .$$

The condition under which the electron is turned back without striking the outer wall, that is, the condition to have magnetic insulation, requires $r_o > r$ so that

$$\ln \frac{r_o}{r_i} > \frac{2\frac{mc^2}{eV_c} \ln \frac{r_o}{r_i}}{\left(\frac{Z_0}{Z_b}\right)^2 - 1}$$

or

$$\frac{Z_b}{Z_0} < \left(\frac{1}{1 + 2\frac{mc^2}{eV}}\right)^{\frac{1}{2}} = \left(\frac{\gamma - 1}{\gamma + 1}\right)^{\frac{1}{2}} \quad .$$

APPENDIX A

Magnetic insulation in vacuum coaxial transmission lines has been the subject of recent investigations by Physics International (PI) and Sandia Laboratories. This work is described in a PI final report.[1]

---

[1] *P. Champney, M. Di Capua, D. Pellinen, and I. D. Smith, Magnetic Insulation in Coaxial Vacuum Transmission Lines, Physics International Co. PIFR-937, San Leandro, CA (January 1977).*

DISTRIBUTION

DEFENSE DOCUMENTATION CENTER
CAMERON STATION, BUILDING 5
ALEXANDRIA, VA 22314
ATTN DDC-TCA (12 COPIES)

COMMANDER
USA RSCH & STD GP (EUR)
BOX 65
FPO NEW YORK 09510
ATTN LTC JAMES M. KENNEDY, JR.
CHIEF, PHYSICS & MATH BRANCH

COMMANDER
US ARMY MATERIEL DEVELOPMENT
& READINESS COMMAND
5001 EISENHOWER AVENUE
ALEXANDRIA, VA 22333
ATTN DRXAM-TL, HQ TECH LIBRARY

COMMANDER
USA MISSILE & MUNITIONS
CENTER & SCHOOL
REDSTONE ARSENAL, AL 35809
ATTN ATSK-CTD-F

DIRECTOR
US ARMY BALLISTIC RESEARCH LABORATORY
ABERDEEN PROVING GROUND, MD 21005
ATTN DRDAR-TSB-S (STINFO)

ASSISTANT TO THE SECRETARY OF DEFENSE
ATOMIC ENERGY
DEPARTMENT OF DEFENSE
WASHINGTON, DC 20301
ATTN ATSD (AE)

DIRECTOR
DEFENSE ADVANCED RESEARCH
PROJECTS AGENCY
ARCHITECT BLDG
1400 WILSON BLVD
ARLINGTON, VA 22209
ATTN DIR, MATERIALS SCIENCES

DIRECTOR
DEFENSE INTELLIGENCE AGENCY
WASHINGTON, DC 20301
ATTN DTICI, ROBERT I. RUBENSTEIN

DIRECTOR
DEFENSE NUCLEAR AGENCY
WASHINGTON, DC 20305
ATTN STVL
ATTN TISI
ATTN TITL
ATTN RAEV

COMMANDER
FIELD COMMAND
DEFENSE NUCLEAR AGENCY
KIRTLAND AFB, NM 87115
ATTN FCPR

DIRECTOR
JOINT STRAT TGT PLANNING STAFF
OFFUTT AFB
OMAHA, NB 68113
ATTN JSAS

CHIEF
LIVERMORE DIVISION FLD COMMAND, DNA
LAWRENCE LIVERMORE LABORATORY
P.O. BOX 808
LIVERMORE, CA 94550
ATTN FCPRL

UNDER SECY OF DEF FOR RSCH & ENGRG
DEPARTMENT OF DEFENSE
WASHINGTON, DC 20301
ATTN S&SS (OS)

COMMANDER
BMD SYSTEM COMMAND
P.O. BOX 1500
HUNTSVILLE, AL 35807
ATTN SSC-TEN

COMMANDER
BALLISTIC MISSILE DEFENSE ADVANCED
TECHNOLOGY CENTER
P.O. BOX 1500
HUNTSVILLE, AL 35807
ATTN ATC-D, LARRY HAVARD

DEP CHIEF OF STAFF FOR RSCH DEV & ACQ
DEPARTMENT OF THE ARMY
WASHINGTON, DC 20310
ATTN DAMA-CSM-N

COMMANDER
REDSTONE SCIENTIFIC INFORMATION CTR
U.S. ARMY R&D COMMAND
REDSTONE ARSENAL, AL 35809
ATTN CHIEF, DOCUMENTS

COMMANDER
US ARMY MISSILE R&D COMMAND
REDSTONE ARSENAL, AL 35809
ATTN DRCPM-PE-EA

DISTRIBUTION (Cont'd)

COMMANDER
US ARMY NUCLEAR & CHEMICAL AGENCY
7500 BACKLICK ROAD
BUILDING 2073
SPRINGFIELD, VA 22150
ATTN LIBRARY

COMMANDER
US ARMY TEST AND EVALUATION COMMAND
ABERDEEN PROVING GROUND, MD 21005
ATTN DRSTE-EL

CHIEF OF NAVAL OPERATIONS
NAVY DEPARTMENT
WASHINGTON, DC 20350
ATTN ROBERT A. BLAISE, 604C4

COMMANDER
NAVAL ELECTRONIC SYSTEMS COMMAND
NAVAL ELECTRONIC SYSTEMS CMD HQS
WASHINGTON, DC 20360
ATTN CODE 5032

COMMANDING OFFICER
NAVAL INTELLIGENCE SUPPORT CTR
4301 SUITLAND ROAD, BLDG 5
WASHINGTON, DC 20390
ATTN NTSC-45

DIRECTOR
NAVAL RESEARCH LABORATORY
WASHINGTON, DC 20375
ATTN GERALD COOPERSTEIN, CODE 7770
ATTN CODE 7701, JACK D. BROWN
ATTN CODE 5410, JOHN DAVIS

OFFICER-IN-CHARGE
NAVAL SURFACE WEAPONS CENTER
WHITE OAK, SILVER SPRING, MD 20910
ATTN CODE WR43
ATTN CODE WA501, NAVY NUC PRGMS OFF

COMMANDER
NAVAL SURFACE WEAPONS CENTER
DAHLGREN, VA 22448
ATTN JERRY FORBES
ATTN F. J. SAZAMA

COMMANDER
NAVAL WEAPONS CENTER
CHINA LAKE, CA 93555
ATTN CODE 533, TECH LIB

AF WEAPONS LABORATORY, AFSC
KIRTLAND AFB, NM 87117
ATTN CA
ATTN NT
ATTN SUL
ATTN DYP

HQ USAF/RD
WASHINGTON, DC 20330
ATTN RDQSM

SAMSO/DY
POST OFFICE BOX 92960
WORLDWAY POSTAL CENTER
LOS ANGELES, CA 90009
(TECHNOLOGY)
ATTN DYS

SAMSO/IN
POST OFFICE BOX 92960
WORLDWAY POSTAL CENTER
LOS ANGELES, CA 90009
(INTELLIGENCE)
ATTN IND, MAJ DARRYL S. MUSKIN

SAMSO/MN
NORTON AFB, CA 92409
(MINUTEMAN)
ATTN MNNH

SAMSO/SK
POST OFFICE BOX 92960
WORLDWAY POSTAL CENTER
LOS ANGELES, CA 90009
(SPACE COMM SYSTEMS)
ATTN SKF, PETER H. STADLER

UNIVERSITY OF CALIFORNIA
LAWRENCE LIVERMORE LABORATORY
P.O. BOX 808
LIVERMORE, CA 94550
ATTN L-18
ATTN L-153
ATTN JOHN NUCKOLLS, A DIV L-545
ATTN TECH INFO DEPT, L-3

SANDIA LABORATORIES
P.O. BOX 5800
ALBUQUERQUE, NM 87115
ATTN DOC CON FOR 3141 SANDIA RPT COLL
ATTN DOC CON FOR 5240 GERALD YONAS

AVCO RESEARCH & SYSTEMS GROUP
201 LOWELL STREET
WILMINGTON, MA 01887
ATTN RESEARCH LIB, A830, RM 7201

BDM CORP
7915 JONES BRANCH DRIVE
MCLEAN, VA 22101
ATTN TECHNICAL LIBRARY

BOEING CO.
P.O. BOX 3707
SEATTLE, WA 98124
ATTN AEROSPACE LIBRARY

DIKEWOOD INDUSTRIES, INC.
1009 BRADBURY DRIVE, S.E.
ALBUQUERQUE, NM 87106
ATTN L. DAVIS

EG&G WASHINGTON ANALYTICAL
SERVICES CENTER, INC.
P.O. BOX 10218
ALBUQUERQUE, NM 87114
ATTN TECHNICAL LIBRARY

FORD AEROSPACE & COMMUNICATIONS CORP
FORD & JAMBOREE ROADS
NEWPORT BEACH, CA 92663
ATTN TECH INFO SECTION

FORD AEROSPACE & COMMUNICATIONS CORP
3939 FABIAN WAY
PALO ALTO, CA 94303
ATTN D. MCMORROW, MS G30
ATTN LIBRARY

GENERAL ELECTRIC CO.
SPACE DIVISION
VALLEY FORGE SPACE CENTER
P.O. BOX 8555
PHILADELPHIA, PA 19101
ATTN J. PEDEN VFSC, 4230M

GENERAL ELECTRIC CO.-TEMPO
CENTER FOR ADVANCED STUDIES
816 STATE STREET (P.O. DRAWER QQ)
SANTA BARBARA, CA 93102
ATTN DASIAC

INSTITUTE FOR DEFENSE ANALYSES
400 ARMY-NAVY DRIVE
ARLINGTON, VA 22202
ATTN IDA LIBRARIAN R. SMITH

ION PHYSICS CORP
SOUTH BEDFORD STREET
BURLINGTON, MA 01803
ATTN H. MILDE

IRT CORP.
P.O. BOX 81087
SAN DIEGO, CA 92138
ATTN R. MERTZ

JAYCOR
1401 CAMINO DEL MAR
DEL MAR, CA 92014
ATTN E. WENAAS

JAYCOR
205 WHITING STREET, SUITE 500
ALEXANDRIA, VA 22304
ATTN R. SULLIVAN

KAMAN SCIENCES CORP.
P.O. BOX 7463
COLORADO SPRINGS, CO 80933
ATTN A. BRIDGES
ATTN J. HOFFMAN
ATTN D. BRYCE
ATTN W. WARE

LOCKHEED MISSILES AND SPACE CO., INC.
3251 HANOVER STREET
PALO ALTO, CA 94304
ATTN LLOYD F. CHASE

MAXWELL LABORATORIES, INC.
9244 BALBOA AVENUE
SAN DIEGO, CA 92123
ATTN A. RICHARD MILLER
ATTN PETER KORN
ATTN ALAN C. KOLB

MCDONNELL DOUGLAS CORP.
5301 BOLSA AVENUE
HUNTINGTON BEACH, CA 92647
ATTN STANLEY SCHNEIDER

MISSION RESEARCH CORP.
735 STATE STREET
SANTA BARBARA, CA 93101
ATTN WILLIAM C. HART
ATTN C. LONGMIRE

MISSION RESEARCH CORP.-SAN DIEGO
P.O. BOX 1209
LA JOLLA, CA 92038
(VICTOR A. J. VAN LINT)
ATTN V. A. J VAN LINT

NORTHROP CORP.
NORTHROP RESEARCH AND TECHNOLOGY CTR
ONE RESEARCH PARK
PALOS VERDES PENN, CA 90274
ATTN LIBRARY

NORTHROP CORP.
ELECTRONIC DIVISION
2301 WEST 120TH STREET
HAWTHORNE, CA 90250
ATTN VINCENT R. DEMARTINO

PHYSICS INTERNATIONAL CO.
2700 MERCED STREET
SAN LEANDRO, CA 94577
ATTN DOC CON FOR BERNARD H. BERNSTEIN
ATTN DOC CON FOR CHARLES H. STALLINGS
ATTN DOC CON FOR PHILIP W. SPENCE
ATTN DOC CON FOR IAN D. SMITH
ATTN DOC CON FOR SIDNEY D. PUTNAM

DISTRIBUTION (Cont'd)

PULSAR ASSOCIATES, INC.
11491 SORRENTO VALLEY BLVD
SAN DIEGO, CA 92121
ATTN CARLETON H. JONES, JR.

R & D ASSOCIATES
P.O. BOX 9695
MARINA DEL REY, CA 90291
ATTN C. MACDONALD
ATTN W. GRAHAM, JR.
ATTN LEONARD SCHLESSINGER

SCIENCE APPLICATIONS, INC.
P.O. BOX 2351
LA JOLLA, CA 92038
ATTN J. ROBERT BEYSTER

SPIRE CORP.
P.O. BOX D
BEDFORD, MA 01730
ATTN ROGER G. LITTLE

SRI INTERNATIONAL
333 RAVENSWOOD AVENUE
MENLO PARK, CA 94025
ATTN SETSUO DAIRIKI

SYSTEMS, SCIENCE & SOFTWARE, INC.
P.O. BOX 1620
LA JOLLA, CA 92038
ATTN ANDREW R. WILSON

TEXAS TECH UNIVERSITY
P.O. BOX 5404 NORTH COLLEGE STATION
LUBBOCK, TX 79417
ATTN TRAVIS L. SIMPSON

TRW DEFENSE & SPACE SYS GROUP
ONE SPACE PARK
REDONDO BEACH, CA 90278
ATTN TECH INFO CENTER/S-1930

VOUGHT CORP.
MICHIGAN DIVISION
38111 VAN DYKE ROAD
STERLING HEIGHTS, MI 48077
ATTN TECH LIB

HARRY DIAMOND LABORATORIES
ATTN COMMANDER/
FLYER, I.N./LANDIS, P.E./
SOMMER, H./OSWALD, R. B.
ATTN CARTER, W.W., DR., TECHNICAL
DIRECTOR
ATTN WISEMAN, ROBERT S., DR., DRDEL-CT
ATTN MARCUS, S. M., 003
ATTN KIMMEL, S., PAO
ATTN CHIEF, 0021
ATTN CHIEF, 0022
ATTN CHIEF, LAB 100
ATTN CHIEF, LAB 200
ATTN CHIEF, LAB 300
ATTN CHIEF, LAB 400
ATTN CHIEF, LAB 500
ATTN CHIEF, LAB 600
ATTN CHIEF, DIV 700
ATTN CHIEF, DIV 800
ATTN CHIEF, LAB 900
ATTN CHIEF, LAB 1000
ATTN RECORD COPY, BR 041
ATTN HDL LIBRARY (5 COPIES)
ATTN CHAIRMAN, EDITORIAL COMMITTEE
ATTN CHIEF, 047
ATTN TECH REPORTS, 013
ATTN PATENT LAW BRANCH, 071
ATTN GIDEP OFFICE, 741
ATTN LANHAM, C., 0021
ATTN CHIEF, 210
ATTN CHIEF 230
ATTN CHIEF 280
ATTN CHIEF 290
ATTN CHIEF 1010
ATTN CHIEF 1020
ATTN CHIEF 1030
ATTN CHIEF 1040
ATTN CHIEF 1050
ATTN GRAYBILL, S. E., (40 COPIES)